Electronic Supplementary Material (ESI) for Physical Chemistry Chemical Physics.

Supporting Information

Investigation of Alkali and Alkaline Earth Solvation Structures in Tetraglyme Solvent

Long Hoang Bao Nguyen [a], Tanguy Picard [b], Nicolas Sergent [b], Christophe Raynaud [a], Jean-Sébastien Filhol [ac*] and Marie-Liesse Doublet [ac*]

[a] ICGM, Univ Montpellier, CNRS, ENSCM, Montpellier, France

[b] Univ. Grenoble Alpes, Univ. Savoie Mont Blanc, CNRS, Grenoble INP, LEPMI, 38000 Grenoble, France

[c] RS2E French Network on Electrochemical Energy Storage, FR5439, Amiens, France

Corresponding authors:

Jean-Sébastien Filhol (Jean-Sebastien.Filhol@umontpellier.fr)

Marie-Liesse Doublet (Marie-Liesse.Doublet@umontpellier.fr)

Experimental and calculation methods

Calculation details. The first coordination sphere of the metal ion and the solvent molecules was constructed and pre-optimised in Avogadro[1], which was then used as input for DFT calculations performed with the Vienna *Ab Initio* Simulation Package (VASP).[2,3] The influence of outer solvent molecules on the first solvation structure was taken into account using a Polarizable Continuum Model (PCM) provided in VASPSOL.[4,5] The PCM is parameterized with the solvent dielectric constant, which is $\varepsilon_r = 7.50$ for G4. DFT calculations were performed within the generalized gradient approximation (GGA) using the Perdew-Burke-Ernzerhof (PBE) functionals[6] for exchange and correlation potential and projector augmented wave pseudopotentials (PAW).[7] The van der Waals interactions were taken into account using the DFT-D3 correction method.[8] Besides the classical GGA functionals, *meta*-GGA functionals, introducing a dependence on the Kohn-Sham orbital kinetic energy density, were also developed to improve the calculation's accuracy. Among all the available *meta*-GGAs, the Strongly Constrained and Appropriately Normed semi-local density functional (SCAN)[9] is the most successful one fulfilling the known constraints of the exact density functional. There is also a strong evidence that the SCAN functional outperforms GGA ones.[10,11] One of the great advantages of SCAN is that the short- and intermediate-range interactions are included in the functional's approximation. The missing long-range interaction, which is important to fully describe van der Waals interactions, can further be added to improve the accuracy of the calculations. In order to compare the efficiency of PBE and SCAN functionals on molecular systems, extra calculations were performed with SCAN, with and without the long-range van der Waals correction. The revised Vydrov-van Voorhis nonlocal correlation functional (rVV10) was used to consider the long-range dispersion interaction.[12–14] All molecular calculations were performed in large unit cells (20 Å × 20 Å × 20 Å) with an energy cut-off of 550 eV at the gamma point. The residual forces after structural relaxation were lower than 0.01 $eV \cdot Å^{-1}$. The charged ions/molecules were generated by removing a corresponding number of electrons from the molecules. The interaction energy between the charged species and the compensating homogeneous background was thus eliminated by extrapolating the size of the unit cell to infinity.[15] The structural visualization was done with VESTA.[16]

Molecular calculations were performed using the Q-Chem code[17], with the pcseg-2 basis set and an electronic convergence of 10^{-8}. Different exchange-correlation functionals, such as PBE, SCAN, hybrid functional PBE0, and range-separated hybrid ωB97M-V, were tested in

this study. The solvent model density (SMD)[18] was used to take into account the effects of the continuum solvent. The SMD of G4 is parametrized with the solvent dielectric constant ε_r = 7.50 and the refractive index of 1.432. The Abraham's hydrogen bond acidity and basicity of G4 are 0 and 0.64, respectively. The bulk surface tension of G4 is 48.88 while its aromaticity and electronegative "halogenicity" are zero.

Sample preparation. Calcium bis (trifluoromethanesulfonyl) imide ($Ca(N(SO_2CF_3)_2)_2$ or $Ca(TFSI)_2$) purchased from TCI Chemical was dried over 48h under vacuum at 80^{o}C and stored in an Ar-filled glovebox. Tetraglyme (≥ 99%) purchased from Merck was distilled under vacuum and kept in an Ar-filled glovebox in molecular sieves to prevent any water contamination. 2 mL solutions of $Ca(TFSI)_2$ in tetraglyme with the concentration 0−0.5 M were prepared to study the solvation structure of Ca^{2+}.

Infrared spectroscopy. The IR spectra were acquired under an inert Ar atmosphere using a Bruker 70v spectrometer. The $Ca(TFSI)_2$/G4 samples were sealed in the IR Omni-Cells, purchased from SPECAC, comprising two transparent KBr windows, which allows the transmission of IR radiation. Each IR spectrum was recorded with a resolution of 2 cm^{-1} and averaged over 128 scans. The measured spectra were referenced to an empty cuvette to eliminate all interferences coming from KBr windows.

In order to verify whether the difference in the choice of basis set may lead to a substantial discrepancy in the structural and energetic values obtained with these two codes, we first compare the enthalpies of the reaction $[M(G4)]^{n+}_{(gas)} + G4_{(gas)} \rightarrow [M(G4)_2]^{n+}_{(gas)}$ (M = Na, K, Mg, and Ca) calculated with the same functionals, e.g. PBE and SCAN, in Q-Chem and VASP codes. In the first stage of the comparison, the implicit solvent model is excluded, and the same input models, pre-optimised with the SCAN functional in the VASP code, are used for all calculations without further structural re-optimisation in order to check the influence of the basis sets on the energetic values. The obtained results reveal a variation of 7–15 $kJ \cdot mol^{-1}$ in the reaction enthalpies obtained at the same level of theory, e.g. PBE and SCAN (Table S1). Such differences are not significant to influence the conclusions that can be drawn from these calculations and set an upper bound of the error due to the choice of the basis set and, to a lower extent, the numerical accuracy of both codes. In the second step, the dispersion correction is added to all calculations, which means the Grimme DFT-D3 correction for PBE and the revised Vydrov-van Voorhis (rVV10) nonlocal correlation functional for the SCAN functional. The resulting enthalpies also show a variation of 6–17 $kJ \cdot mol^{-1}$ between the two codes for the same level of theory. It is important to note that the inclusion of the dispersion correction significantly impacts the reaction enthalpies (Table S1); thus, indicating the importance of the van der Waals interactions in these systems and the necessity to include them in the calculations. Many previous studies have pointed out that the newly developed SCAN-rVV10 outperforms the conventional PBE-D3 functional in the structural optimisation and the electronic structure calculations [9,10]; nevertheless, when one carefully examines the reaction enthalpies, as in this study, both functionals result in equivalent data. When more complicated basis set in Q-Chem code, such as pcseg-3, is used, greater agreement is observed in the energetic values obtained with the two codes (Table S2). Nonetheless, in order to ensure a compromise between the calculation time and the efficiency of the calculations, the pcseg-2 basis set is used in further molecular calculations performed with Q-Chem code. The energetic values are also calculated when the input structures were re-optimised at the same theory level before the energy calculation step, and the obtained results are gathered in Table S3. As previously, both codes lead to energies lying in the same range of the systematic error caused in particular by the difference in the choice of the basis sets.

The implicit solvent model is now introduced in all calculations, and the reaction enthalpies are calculated without (Table S4) and with structural re-optimisation (Table S5). In both cases, the reaction enthalpies calculated in the presence of the implicit solvent model at the same level

of theory in the two codes show a difference of 10–20 kJ·mol^{-1}, which is again very close to the systematic error discussed above. Despite the difference in the basis sets and the implicit solvent model models employed in the two codes, the molecular modelling performed in Q-Chem and VASP codes both produce equivalent geometric and energetic information, showing that the difference in the reaction enthalpies mainly come from the choice of the functionals. The calculations performed with functionals lying at higher rungs in the Jacob's ladder, such as the hybrid functional PBE0-D3BJ and the range-separated hybrid ωB97M-V, do not lead to substantial changes in the reaction enthalpies (Table S5).

Table S1. Enthalpy of the reaction $[M(G4)]^{n+}_{(gas)} + G4_{(gas)} \rightarrow [M(G4)_2]^{n+}_{(gas)}$ (M = Na, K, Mg, and Ca) calculated with different functionals in Q-Chem and VASP codes on the structures pre-optimised with the SCAN functional in the VASP code. The pcseg-2 basis set was used in the Q-Chem calculations.

M^{n+}	ΔH° (kJ·mol^{-1})							
	Q-Chem				VASP			
	PBE	PBE-D3	SCAN	SCAN-rVV10	PBE	PBE-D3	SCAN	SCAN-rVV10
Na^+	-41	-121	-91	-119	-34	-114	-81	-109
K^+	-34	-98	-68	-93	-26	-90	-59	-84
Mg^{2+}	-176	-245	-223	-247	-168	-237	-208	-241
Ca^{2+}	-208	-287	-272	-301	-200	-270	-264	-293

Table S2. Enthalpy of the reaction $[M(G4)]^{n+}_{(gas)} + G4_{(gas)} \rightarrow [M(G4)_2]^{n+}_{(gas)}$ (M = Na, K, Mg, and Ca) calculated with different functionals in Q-Chem and VASP codes on the structures pre-optimised with the SCAN functional in the VASP code. The pcseg-3 basis set was used in the Q-Chem calculations.

M^{n+}	ΔH° (kJ·mol^{-1})							
	Q-Chem				VASP			
	PBE	PBE-D3	SCAN	SCAN-rVV10	PBE	PBE-D3	SCAN	SCAN-rVV10
Na^+	-36	-115	-86	-113	-34	-114	-81	-109
K^+	-30	-93	-64	-88	-26	-90	-59	-84
Mg^{2+}	-167	-237	-215	-239	-168	-237	-208	-241
Ca^{2+}	-200	-278	-263	-292	-200	-270	-264	-293

Table S3. Enthalpy of the reaction $[M(G4)]^{n+}_{(gas)} + G4_{(gas)} \rightarrow [M(G4)_2]^{n+}_{(gas)}$ (M = Na, K, Mg, and Ca) calculated with different functionals in Q-Chem and VASP codes. The input structures were re-optimised at the same level of theory before the energetic calculations. The pcseg-2 basis set was used in the Q-Chem calculations.

M^{n+}	ΔH° (kJ·mol^{-1})							
	Q-Chem				VASP			
	PBE	PBE-D3	SCAN	SCAN-rVV10	PBE	PBE-D3	SCAN	SCAN-rVV10
Na^+	-57	-116	-92	-121	-47	-118	-81	-111
K^+	-52	-108	-77	-102	-39	-94	-59	-84
Mg^{2+}	-199	-247	-223	-248	-177	-238	-208	-249
Ca^{2+}	-244	-292	-276	-308	-208	-280	-264	-291

Table S4. Enthalpy of the reaction $[M(G4)]^{n+}_{(PCM)} + G4_{(PCM)} \rightarrow [M(G4)_2]^{n+}_{(PCM)}$ (M = Na, K, Mg, and Ca) calculated with different functionals in Q-Chem and VASP codes with the inclusion of the PCM model. The input models were pre-optimised with the SCAN functional in the VASP code. No structural reoptimisation was applied on the input models. The pcseg-2 basis set was used in the Q-Chem calculations.

M^{n+}	ΔH° (kJ·mol^{-1})							
	Q-Chem				VASP			
	PBE	PBE-D3	SCAN	SCAN-rVV10	PBE	PBE-D3	SCAN	SCAN-rVV10
Na^+	-9	-88	-58	-85	-19	-99	-66	-94
K^+	-3	-67	-37	-61	-7	-70	-39	-64
Mg^{2+}	-75	-144	-120	-145	-91	-161	-139	-164
Ca^{2+}	-127	-205	-190	-218	-121	-199	-185	-214

Table S5. Enthalpy of the reaction $[M(G4)]^{n+}_{(PCM)} + G4_{(PCM)} \rightarrow [M(G4)_2]^{n+}_{(PCM)}$ (M = Na, K, Mg, and Ca) calculated with different functionals in Q-Chem and VASP codes with the inclusion of the implicit solvent model. The input models were reoptimised at the same level of theory before the energetic calculations. The pcseg-2 basis set was used in the Q-Chem calculations.

M^{n+}	ΔH° (kJ·mol^{-1})									
	Q-Chem						VASP			
	PBE	PBE-D3	SCAN	SCAN-rVV10	PBE0-D3BJ	B97M-V	PBE	PBE-D3	SCAN	SCAN-rVV10
Na^+	-12	-79	-59	-85	-70	-77	-31	-98	-66	-97
K^+	-26	-81	-52	-73	-67	-80	-17	-72	-39	-64
Mg^{2+}	-91	-150	-125	-150	-148	-157	-96	-161	-138	-159
Ca^{2+}	-143	-201	-192	-221	-208	-233	-126	-199	-186	-209

Table S6. Selected geometry data for the structure of *cis*- and *trans*-$TFSI^-$ optimised using the PBE-D3 and SCAN-rVV10 functionals with the presence of the PCM in the VASP code.

	***cis*-TFSI$^-$**		***trans*-TFSI$^-$**	
	PBE-D3	SCAN-rVV10	PBE-D3	SCAN-rVV10
S−N (Å)	1.59 × 2	1.57 × 2	1.59 × 2	1.57 × 2
S−O (Å)	1.45 × 4	1.43 × 4	1.45 × 4	1.43 × 4
S−C (Å)	1.88	1.84	1.88 × 2	1.84 × 2
	1.89	1.85		
C−F (Å)	1.36 × 6	1.34 × 2	1.36 × 6	1.34 × 2
		1.35 × 4		1.35 × 4
S−N−S (°)	127.7	126.8	126.3	126.3
C−S−S−C (°)	33.0	37.3	178.8	179.3

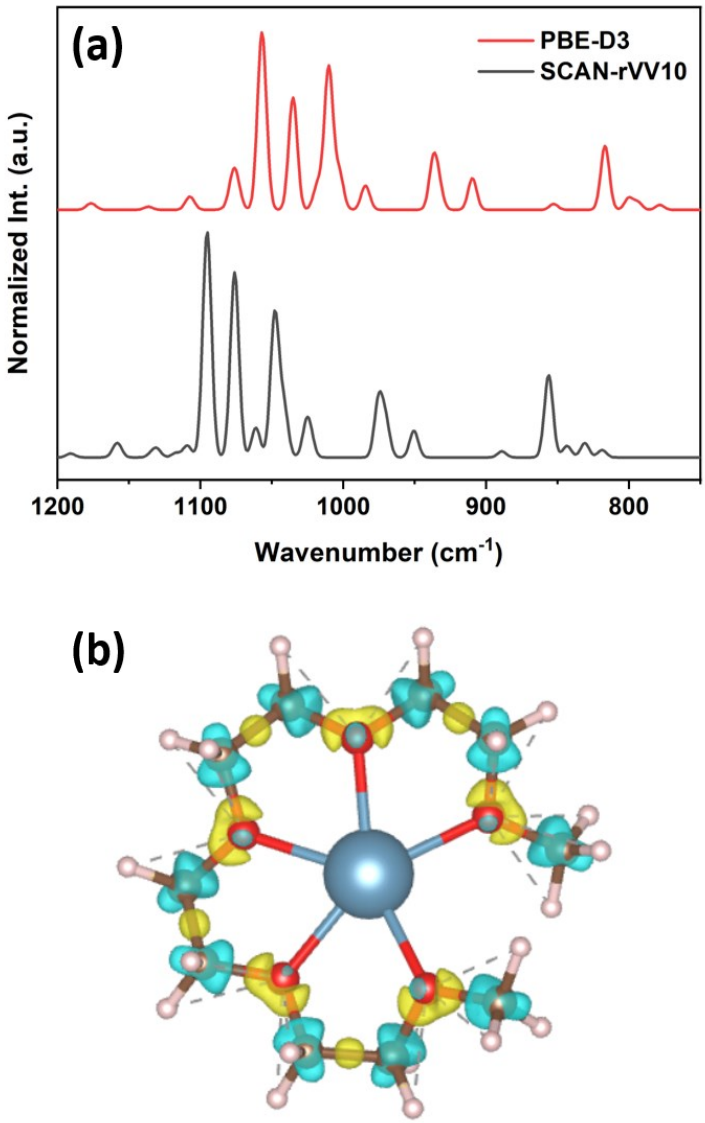

Figure S1. (a) Comparison of IR spectra in the 750−1200 cm^{-1} range of $[Ca(G4)]^{2+}$ computed with SCAN-rVV10 and PBE-D3 functionals embedded in the VASP code. (b) Charge density difference at an iso-surface density of $3.5 \cdot 10^{-3}$ electron·$Å^{-2}$ of $[Ca(G4)]^{2+}$ calculated with SCAN-rVV10 and PBE-D3 functionals in the VASP code with the PCM inclusion. The yellow and blue colours indicate the areas where the electron density is enhanced or depleted in the SCAN-rVV10 functional.

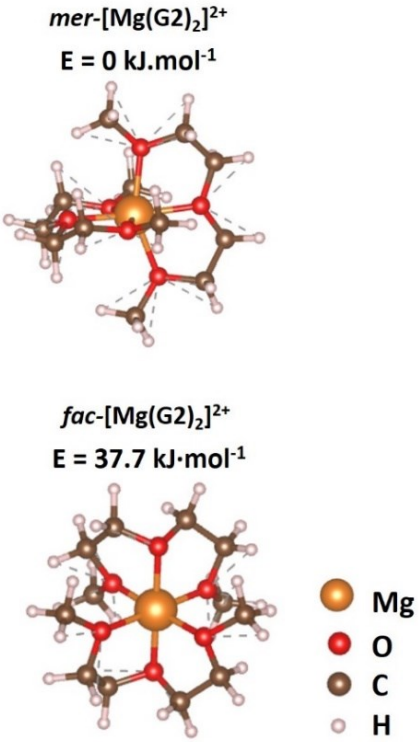

Figure S2. Optimised structures and the relative energy of *mer*- and *fac*-$[Mg(G2)_2]^{2+}$ isomers calculated with the SCAN-rVV10 functional.

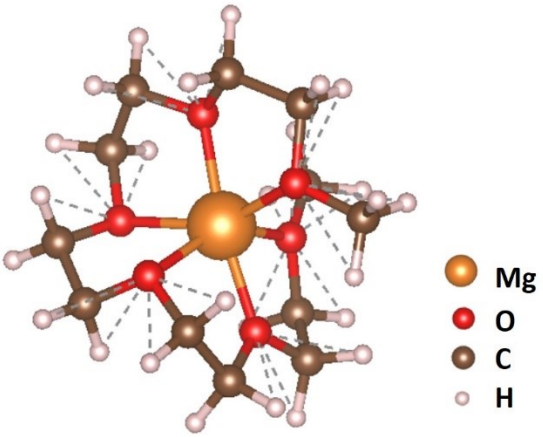

Figure S3. The solvation structure of $[Mg(G5)]^{2+}$ calculated with the SCAN+rVV10 function in the VASP code.

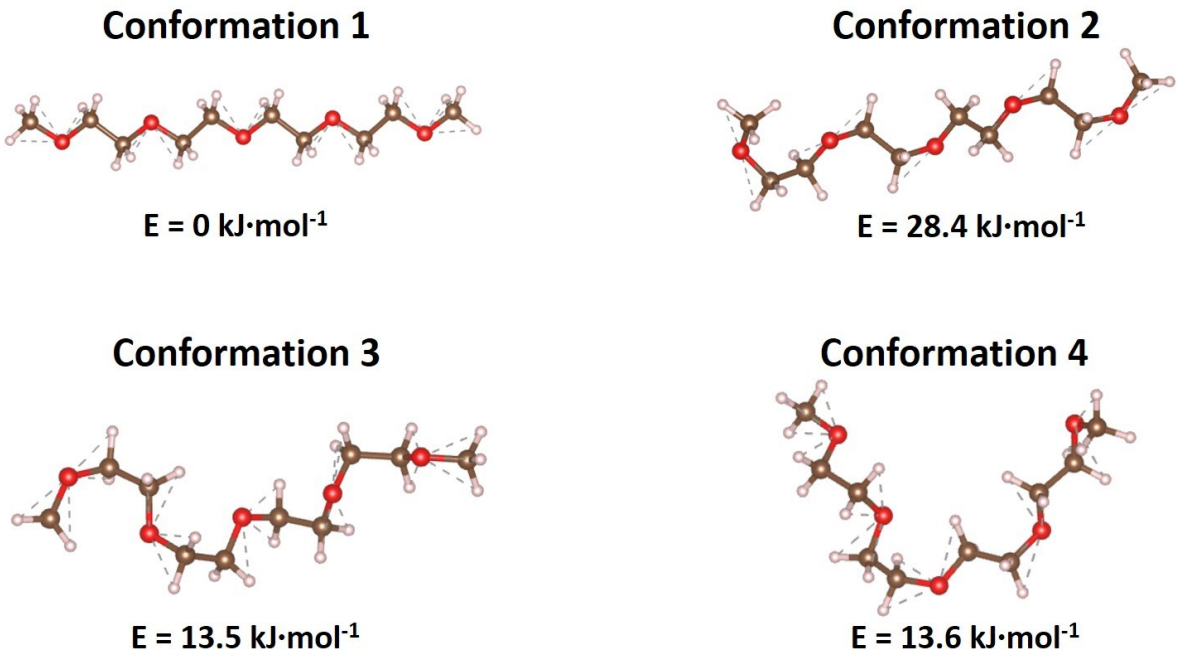

Figure S4. The four representative conformations of G4 molecule and their relative energies.

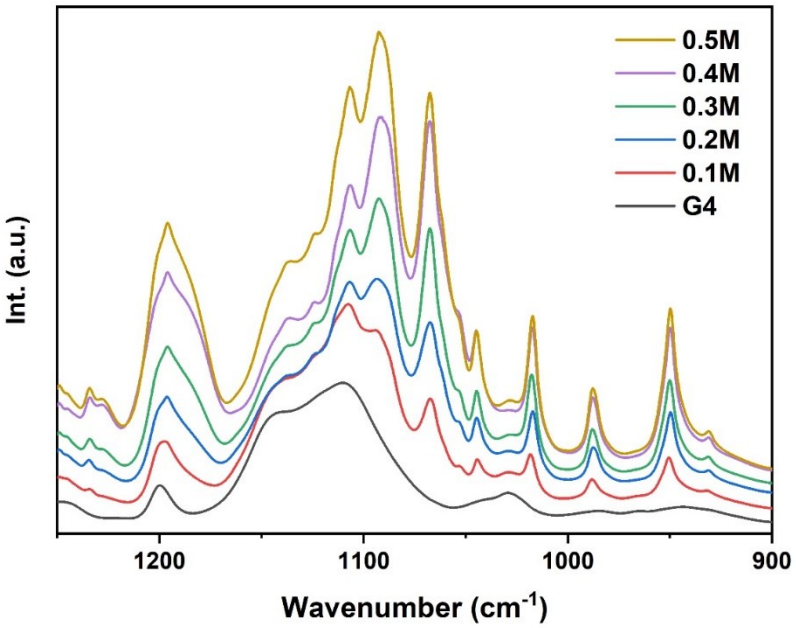

Figure S5. Experiment IR spectra acquired on $Ca(TFSI)_2$ solution in G4 with the concentration range 0−0.5 M.

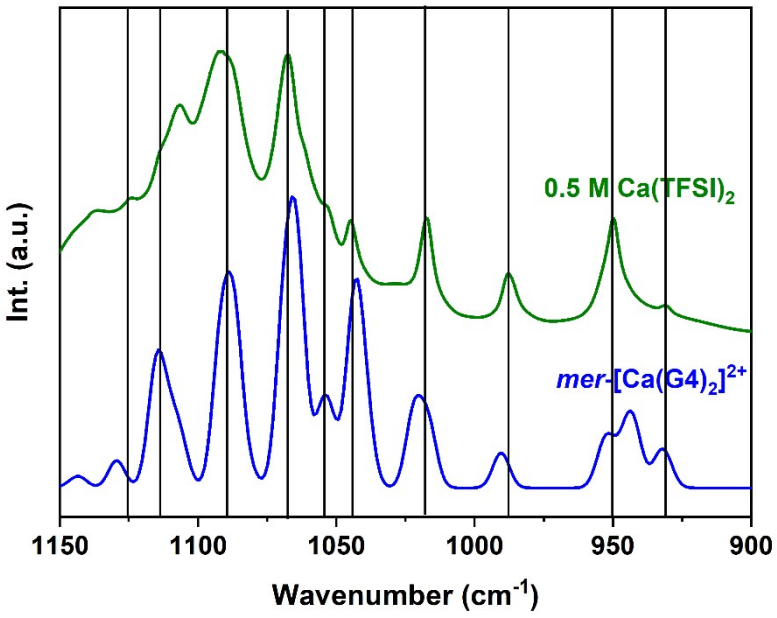

Figure S6. Comparison between the experimental IR spectrum recorded on a 0.5 $Ca(TFSI)_2$/G4 solution and the IR spectrum of *mer*-$[Ca(G4)_2]^{2+}$ computed by the SCAN-rVV10 functional available in the VASP code. A scaling factor of 0.986 was applied on the computed spectrum.

References:

1 M. D. Hanwell, D. E. Curtis, D. C. Lonie, T. Vandermeersch, E. Zurek and G. R. Hutchison, Avogadro: an advanced semantic chemical editor, visualization, and analysis platform, *J. Cheminform.*, 2012, **4**, 17.

2 G. Kresse and J. Furthmüller, Efficiency of ab-initio total energy calculations for metals and semiconductors using a plane-wave basis set, *Comput. Mater. Sci.*, 1996, **6**, 15–50.

3 G. Kresse and J. Furthmüller, Efficient iterative schemes for ab initio total-energy calculations using a plane-wave basis set, *Phys. Rev. B - Condens. Matter Mater. Phys.*, 1996, **54**, 11169–11186.

4 M. Fishman, H. L. Zhuang, K. Mathew, W. Dirschka and R. G. Hennig, Accuracy of exchange-correlation functionals and effect of solvation on the surface energy of copper, *Phys. Rev. B*, 2013, **87**, 245402.

5 K. Mathew, R. Sundararaman, K. Letchworth-Weaver, T. A. Arias and R. G. Hennig, Implicit solvation model for density-functional study of nanocrystal surfaces and reaction pathways, *J. Chem. Phys.*, 2014, **140**, 0–8.

6 J. P. Perdew, K. Burke and M. Ernzerhof, Generalized gradient approximation made simple, *Phys. Rev. Lett.*, 1996, **77**, 3865–3868.

7 G. Kresse and D. Joubert, From ultrasoft pseudopotentials to the projector augmented-wave method, *Phys. Rev. B*, 1999, **59**, 1758–1775.

8 S. Grimme, J. Antony, S. Ehrlich and H. Krieg, A consistent and accurate ab initio parametrization of density functional dispersion correction (DFT-D) for the 94 elements H-Pu, *J. Chem. Phys.*, , DOI:10.1063/1.3382344.

9 J. Sun, A. Ruzsinszky and J. Perdew, Strongly Constrained and Appropriately Normed Semilocal Density Functional, *Phys. Rev. Lett.*, 2015, **115**, 1–6.

10 J. H. Yang, D. A. Kitchaev and G. Ceder, Rationalizing accurate structure prediction in the meta-GGA SCAN functional, *Phys. Rev. B*, 2019, **100**, 1–10.

11 J. Sun, R. C. Remsing, Y. Zhang, Z. Sun, A. Ruzsinszky, H. Peng, Z. Yang, A. Paul, U. Waghmare, X. Wu, M. L. Klein and J. P. Perdew, Accurate first-principles structures and energies of diversely bonded systems from an efficient density functional, *Nat. Chem.*, 2016, **8**, 831–836.

12 H. Peng, Z. H. Yang, J. P. Perdew and J. Sun, Versatile van der Waals density functional based on a meta-generalized gradient approximation, *Phys. Rev. X*, 2016, **6**, 1–15.

13 J. Klimeš, D. R. Bowler and A. Michaelides, Van der Waals density functionals applied to solids, *Phys. Rev. B*, 2011, **83**, 195131.

14 J. Klimeš, D. R. Bowler and A. Michaelides, Chemical accuracy for the van der Waals density functional, *J. Phys. Condens. Matter*, 2010, **22**, 022201.

15 A. K. Lautar, J. Bitenc, R. Dominko and J. S. Filhol, Building Ab Initio Interface Pourbaix diagrams to Investigate Electrolyte Stability in the Electrochemical Double Layer: Application to magnesium batteries, *ACS Appl. Mater. Interfaces*, 2021, **13**, 8263–8273.

16 K. Momma and F. Izumi, VESTA: A three-dimensional visualization system for electronic and structural analysis, *J. Appl. Crystallogr.*, 2008, **41**, 653–658.

17 Y. Shao, Z. Gan, E. Epifanovsky, A. T. B. Gilbert, M. Wormit, J. Kussmann, A. W. Lange, A. Behn, J. Deng, X. Feng, D. Ghosh, M. Goldey, P. R. Horn, L. D. Jacobson, I. Kaliman, R. Z. Khaliullin, T. Kuś, A. Landau, J. Liu, E. I. Proynov, Y. M. Rhee, R. M. Richard, M. A. Rohrdanz, R. P. Steele, E. J. Sundstrom, H. L. Woodcock,

P. M. Zimmerman, D. Zuev, B. Albrecht, E. Alguire, B. Austin, G. J. O. Beran, Y. A. Bernard, E. Berquist, K. Brandhorst, K. B. Bravaya, S. T. Brown, D. Casanova, C. M. Chang, Y. Chen, S. H. Chien, K. D. Closser, D. L. Crittenden, M. Diedenhofen, R. A. Distasio, H. Do, A. D. Dutoi, R. G. Edgar, S. Fatehi, L. Fusti-Molnar, A. Ghysels, A. Golubeva-Zadorozhnaya, J. Gomes, M. W. D. Hanson-Heine, P. H. P. Harbach, A. W. Hauser, E. G. Hohenstein, Z. C. Holden, T. C. Jagau, H. Ji, B. Kaduk, K. Khistyaev, J. Kim, J. Kim, R. A. King, P. Klunzinger, D. Kosenkov, T. Kowalczyk, C. M. Krauter, K. U. Lao, A. D. Laurent, K. V. Lawler, S. V. Levchenko, C. Y. Lin, F. Liu, E. Livshits, R. C. Lochan, A. Luenser, P. Manohar, S. F. Manzer, S. P. Mao, N. Mardirossian, A. V. Marenich, S. A. Maurer, N. J. Mayhall, E. Neuscamman, C. M. Oana, R. Olivares-Amaya, D. P. Oneill, J. A. Parkhill, T. M. Perrine, R. Peverati, A. Prociuk, D. R. Rehn, E. Rosta, N. J. Russ, S. M. Sharada, S. Sharma, D. W. Small, A. Sodt, T. Stein, D. Stück, Y. C. Su, A. J. W. Thom, T. Tsuchimochi, V. Vanovschi, L. Vogt, O. Vydrov, T. Wang, M. A. Watson, J. Wenzel, A. White, C. F. Williams, J. Yang, S. Yeganeh, S. R. Yost, Z. Q. You, I. Y. Zhang, X. Zhang, Y. Zhao, B. R. Brooks, G. K. L. Chan, D. M. Chipman, C. J. Cramer, W. A. Goddard, M. S. Gordon, W. J. Hehre, A. Klamt, H. F. Schaefer, M. W. Schmidt, C. D. Sherrill, D. G. Truhlar, A. Warshel, X. Xu, A. Aspuru-Guzik, R. Baer, A. T. Bell, N. A. Besley, J. Da Chai, A. Dreuw, B. D. Dunietz, T. R. Furlani, S. R. Gwaltney, C. P. Hsu, Y. Jung, J. Kong, D. S. Lambrecht, W. Liang, C. Ochsenfeld, V. A. Rassolov, L. V. Slipchenko, J. E. Subotnik, T. Van Voorhis, J. M. Herbert, A. I. Krylov, P. M. W. Gill and M. Head-Gordon, Advances in molecular quantum chemistry contained in the Q-Chem 4 program package, *Mol. Phys.*, 2015, **113**, 184–215.

18 A. V. Marenich, C. J. Cramer and D. G. Truhlar, Universal solvation model based on solute electron density and on a continuum model of the solvent defined by the bulk dielectric constant and atomic surface tensions, *J. Phys. Chem. B*, 2009, **113**, 6378–6396.